

We are IntechOpen, the world's leading publisher of Open Access books Built by scientists, for scientists

6,900

Open access books available

185,000

International authors and editors

200M

Downloads

Our authors are among the

154

Countries delivered to

TOP 1%

most cited scientists

12.2%

Contributors from top 500 universities



WEB OF SCIENCE™

Selection of our books indexed in the Book Citation Index
in Web of Science™ Core Collection (BKCI)

Interested in publishing with us?
Contact book.department@intechopen.com

Numbers displayed above are based on latest data collected.
For more information visit www.intechopen.com



Experimental Study on Generation of Single Cavitation Bubble Collapse Behavior by a High Speed Camera Record

Sheng-Hsueh Yang¹, Shenq-Yuh Jaw² and Keh-Chia Yeh¹

¹*National Chiao Tung University Hsinchu, Taiwan,*

²*National Taiwan Ocean University Keelung, Taiwan, R.O.C.*

1. Introduction

It has been known that the collapse of the cavitation bubbles could cause serious destruction of pressure pipes, hydraulic machineries and turbine structures. After the cavitation bubble is generated, the variation of its surrounding velocity and pressure field could result in its collapse. If the process of the collapse of a cavitation bubble appears near the solid boundary, its impact to the boundary could generate an immense water-hammer pressure effect (Plesset and Chapman, 1971). The shock wave generated in this process of bubble collapse could possibly impact or even destroy the solid boundary of structure. The bubble collapse studies include the understanding of the shock wave, the characteristics of the resultant luminescence, and the jet related fields. If the cavitation bubble is located near the solid boundary at certain suitable distance, it is more possible for the production of counter-jet in the process of bubble collapse. There has not been a firm conclusion for the exact characteristics which causes the destruction of the interface on the solid boundary.

Rayleigh (1917) studied the corrosion of high speed blade subjected to the effect of cavitation bubble. He mentioned that the bubble collapse is able to produce a high speed flow jet which damages the solid surface. Plesset (1949) further considered the influence of the physical characteristics of fluid viscosity and surface tension and derived the Rayleigh-Plesset equation. Kornfeld and Suvorov (1944) brought up the theory of bubble collapse near a solid boundary. They proposed that the bubble would be deformed to a non-spherical shape with the bubble surface tension penetrated subsequently to generate the phenomenon of flow jet. This phenomenon was proved in the experiment carried out by Naude and Ellis (1961). The numerical model in Plesset and Chapman's research (1971) also revealed this phenomenon. If the solid boundary is located on the right side of the bubble, the jet flow would be formed on the left side of the bubble and penetrates it before arriving at the right side interface of the bubble. The damage of the solid boundary might be caused by the impact of this jet flow during the bubble collapse. Benjamin and Ellis (1966) and Philipp and Lauterborn (1998) also detected the bubble collapse phenomenon and its consequent behavior of damage at the solid boundary. Recent research results revealed that the destructive power of the jet flow was not the main factor for the damage of the solid

boundary. However, the jet flow influence which causes the collapse of the bubble is still an important element for the research of the hydrodynamics of the flow field.

Rayleigh (1917) first analyzed the theoretical pressure variation of the flow field of the bubble collapse. The bubble collapse results in a very high pressure, forming a shock wave which is sent towards the outside of the bubble. Harrison (1952) in his experimental results proved the existence of a noise generated by the collapse of bubble at its surrounding rigid boundary. Vogel and Lauterborn (1988) found a close relationship between the strength of the wave pulse and the distance between the position of the bubble and the rigid boundary. This wave pulse could then generate a series of shock waves. This phenomenon was studied and revealed in the experiments carried out by Tomita and Shima (1986); Ward and Emmony (1991); Ohl et al.; Shaw et al. (1995); Lindau and Lauterborn (2003).

Light could be emitted in the process of the bubble collapse when the volume of the bubble is compressed to its minimum radius during which the gas inside is heated in a heat-insulated process. For bubbles under low viscosity and high pressure, it is easier for the emission of light. This is because at high viscosity, the time for bubble collapse is increased and the gas inside is not heated to the sufficient temperature to emit light. Ohl et al. (1998) also found the emission of light near the solid boundary under specific conditions in the process of bubble collapse. This phenomenon is called the "Single Cavitation Bubble Luminescence (SCBL)". Buzukov and Teslenko (1971) and Akmanov et al. (1974) also had similar research reports.

Counter jet could be generated when the bubble is located near the solid boundary. The initial formation and increment of the size of the counter jet is very rapid and it could exist for a while. Experiments related to the counter jet are found in Harrison (1952) and Kling and Hammitt's (1972) researches but it is until Lauterborn (1974) who first described the counter jet phenomenon. There has not been a final conclusion for the cause of the generation of the counter jet. Counter jet did not appear in the numerical simulations carried out by Best (1993); Zhang et al. (1993); Blake et al. (1997). However, it appeared in the experiments carried out by Tomita and Shima (1986); Vogel et al. (1989); Ward and Emmony (1991); Philipp and Lauterborn (1998); Kodama and Tomita (2000). The discrepancy between the numerical simulations and the experimental results leads to the assumption that the counter jet flow field is not part of the bubble collapse process. Its formation might be generated by a complicated mechanism in the fluid during the bubble collapse. For example, if the bubble is in contact with the solid boundary, the counter jet would not be generated. The shock wave generated appears at the final stage of the process of bubble collapse. Since the counter jets also appear at the final stage of the bubble collapse, there are speculations for their possible formation due to the shock wave structure.

According to Rayleigh's equation, when the effect of the surrounding solid boundary is excluded, the relationship between the time of bubble collapse and its radius is:

$$R_{\max} = 1.09 \sqrt{\frac{p - p_v}{\rho}} t_c \quad (1)$$

where R_{\max} is the maximum radius, p and ρ are the pressure of the flow field and the fluid density at ambient temperature respectively, p_v is the vapor pressure, t_c is the bubble

collapse time. If the solid boundary condition is put into consideration, a greater bubble collapse time is required. Generally the size of the cavitation bubble produced in the laboratory is about 1.5 mm in radius. Under ambient temperature, the bubble collapse time ranges from $100\mu\text{s} \sim 200\mu\text{s}$. It is not easy to generate cavitation bubbles for their small volumes, short collapse time, and complicated flow fields; all of which contribute to a great difficulty of the measurement. In order to record and analyze the characteristics of the flow field of the bubble collapse, common experimental setup includes a high speed camera with framing rates ranging between several thousand to 100 million frames per second. Some researchers used the method of particle image velocimetry (PIV) to measure the velocity flow field of the process of bubble collapse (Vogel et al., 1989). However since the volume of the bubble was small and its collapse time was too short, only a rough sketch of the flow field was obtained. Lawson et al. (1999) applied the PIV method to measure the flow field of the collapse of a 80 mm diameter rubber balloon and compared it with the numerical simulation. Although these results obtained agreement, there is great discrepancy between the flow field features of the collapse of a balloon and a bubble. Jaw et al. (2007) obtained sound experimental results using soap bubbles filled with smog particle and applied the PIV method to measure flow fields at different phases during the process of bubble collapse.

In laboratory, a single cavitation bubble could be generated in a test tube using a high energy laser beam to focus on a single point (Lauterborn, 1972). In the following years, many related studies utilized this method to generate a single cavitation bubble. Since these bubbles were generated by the high energy laser beam which causes fluid aeration, it was restricted by the strength of the energy provided by the laser. Usually the bubble created using this method has small volume with 1.5 mm in radius. In addition, the inside pressure of the bubble was not equivalent to the vapor pressure at ambient temperature. Moreover, since the bubbles were formed by fluid aeration which parted the fluid molecules, there is no re-congealable vapor inside the bubbles to repeat the experiment. Some other researchers used the method of electrolysis to generate a bubble on a platinum electrode at the bottom of a box. However, this method has a defect of disturbing the flow field during the bubble collapse. Another method for forming the bubble is through the use of a needle to inject air into the test tube before using a lithotripter to generate a shock wave up to 94 MPa to break the bubble (Philipp et al.1993). Sankin et al.(2005) also used a lithotripter to generate a 39 MPa shock wave to break the laser induced bubble in order to measure the flow field of the interaction between the bubble collapse and the shock wave.

From the paper reviews presented above, it is perceived that the cavitation bubble collapse flow is very difficult to measure due to the facts that the bubble size is small, the collapse time is very short, and the flow induced is very complicate. In addition, as mentioned before, the bubble generated by the optical breakdown is different from a true cavitation bubble. A cavitation bubble containing re-condensable vapor, when collapsed, will produce greater energy than the ones without re-condensable vapor (Zhu and Zhong, 1999). To resolve these problems, a simpler method for the generation of a true cavitation bubble is proposed in this study. By rotating a L tube filled with tap water, a single cavitation bubble is generated and stayed at the center of the rotational axis due to the effect of centrifugal force. The cinematographic analysis of bubble collapse flows induced by pressure waves of different strengths can thus be performed easily. By lowering the strength of the pressure wave, the bubble collapsed in a longer period of time, the characteristics of the true

cavitation bubble collapse flow are clearly manifested. Improvement in the further used the PIV method that can be clear revealed velocity flow field feature during the bubble collapse. The present study focuses on the investigation of the formation of the liquid jet and the counter jet, at different stand-off distances to the boundary, and their consequent influences on the bubble collapse flow.

2. Experiment Instrument and cavitation bubble generator

The experimental setup for the flow field measurement of cavitation bubble collapse is shown in Figure 1. This device is consisted of an insulated optical platform, a motor, a rotatable U-shape platform, a transparent cylindrical tube, a set of light sources, a shock wave pressure generator, a high speed camera and a pressure sensor. The DC brushless motor is capable to produce a maximum controlled rotational velocity up to 2,000 RPM, to supply a maximum power up to two horsepower, and to stop the rotational motion in a relatively short period of time.

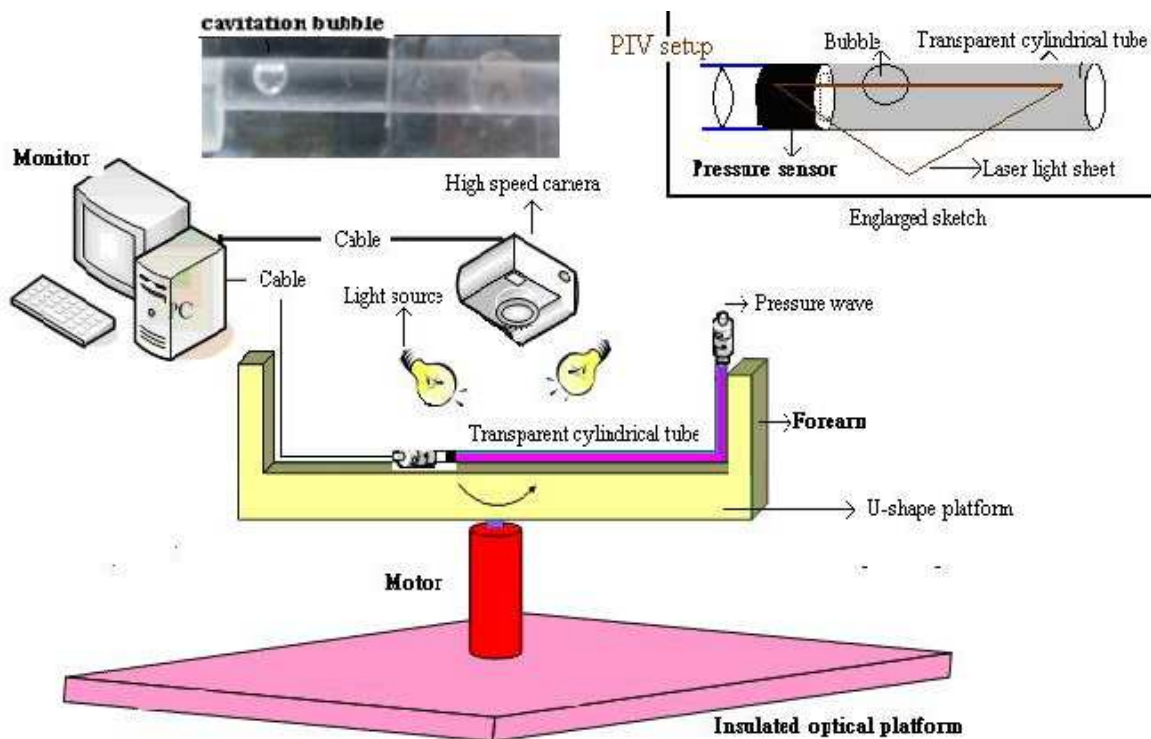


Fig. 1. Schematic diagram of the experiment setup.

The U-shape platform was made up of an acrylic platform of 20 mm in thickness. Centered at the rotational axis of the motor, its rotatable arm has a radius of 250 mm, which resulted in a total horizontal length of 500 mm. Two vertical forearms each of 150 mm in height are fixed to the edge of the platform. On the platform of the horizontal rotatable level arm sites the transparent cylindrical tube of 200 mm in length, with its internal and external diameter of 5mm and 8mm respectively. A soft PVC tube with an internal diameter of 5mm is fixed to the vertical forearm in order to conveniently exchange the experimental equipment. At one end, this tube is connected to the shock wave pressure generator with a piston while it is extended to connect the transparent cylindrical tube at the other end. At the extremity of the transparent cylindrical tube, a rigid boundary with a 1 mm drilled hole is set up to connect

the highly sensitive pressure sensor that measures the shock wave pressure at different strengths during the process of the single bubble collapse (shown at the upper part of Figure 1). On the other hand, the cavitation bubble generation takes place at the site on the platform of the rotational axis where the pressure is at the lowest. Therefore, the transparent cylindrical tube must be located across the center of the rotational axis for easier cavitation bubble generation.

During the experiment of generating a single cavitation bubble, the transparent cylindrical tube on the U-shape platform is filled with tap water shown in Figure 2. The surface of the fluid at the part of the vertical forearm tube is in touch with air with one atmosphere pressure. Therefore, the center location of the L tube at initial condition has a hydrostatic pressure of p_0

$$p_0 = p_{atm} + \rho g \Delta h, \quad (2)$$

where p_{atm} is the atmosphere pressure, g is the acceleration of gravity, and Δh is the water depth difference.

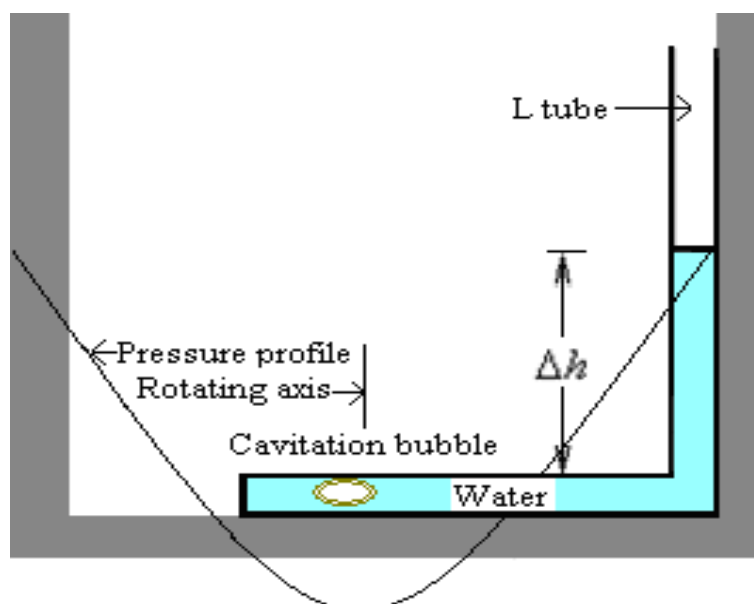


Fig. 2. The pressure distribution for a rotating U-shape platform.

When the U-shape platform is rotated by the motor, the fluid is subjected to a centrifugal force resulting in a parabolic fluid pressure distribution shown as the solid line in Figure 2 at different radius. At the vertical forearm, although the Δh is slightly increased, the hydrostatic water pressure is still kept at one atmospheric pressure because the surface interface is still in touch with the air. Therefore, the pressure difference between the free surface atmospheric pressure and the pressure at the center of rotation is p_c

$$P_c = \rho g \Delta h - 1/2 \rho r^2 \omega^2, \quad (3)$$

where r is the rotational radius and ω is the rotational velocity. When ω is gradually increased, the pressure at the center of the rotation in the transparent cylindrical tube is gradually decreased to a saturated vapor pressure at local present water temperature. At this condition, a single cavitation bubble at the rotational center can be generated. The

rotational speed needed for generating a cavitation bubble is related to the Δh . Greater Δh means a greater rotational velocity required for the production of cavitation bubble. If Δh is kept constant, an increasing rotational velocity would result in a greater size of cavitation bubble. Therefore by controlling the rotational velocity of the U-shape platform, a desirable size of a single cavitation bubble could be generated.

After the cavitation bubble is generated, the U-shape platform is stopped to restore the pressure back to the hydrostatic pressure instantly. This pressure difference alone is not enough to break the cavitation bubble. Therefore, in order to observe the flow field of the collapse of the cavitation bubble, this study uses a pulse setup to hit the piston of the PVC soft tube in contact with the free water surface and instantly generates a shock wave pressure sending an impact to cause the collapse of the cavitation bubble. The signal to propel the pulse setup impacting the piston device is triggered while the image data and the pressure profile are recorded and stored by the computer through the high speed camera and the pressure sensor respectively. This experimental setup allows the real-time recording of the time-series relationships between the flow field image data and the pressure change profile with their subsequent analysis.

A Fastec high speed camera is used to extract and record the experimental images. The speed of image extraction is determined by the size of the image. For example, an image extraction speed of 4,000 frame /second is used for an image size of 1280×128 pixels. A Kulite XTL-190 pressure sensor incorporating with the NI-6221 Analog I/O device are used for the measurement of the pressure profile. The NI-6221 Analog I/O device can send a 10 V signal to drive the pressure sensor and receive a 0 – 0.5 V pressure signal to record data which enables itself for the analysis of the pressure change profile in the transparent cylindrical tube.

On the other hand, PIV method is used Argun laser pass a transparent cylindrical glass to form a light sheet and in the liquid arranged TSI glass bead-hollow particle (8-12 μ m) to assist the camera catch the particle image during the cavitation bubble collapse process, as shown in upper right schematic diagram in Figure 1. The light sheet thickness is 1.5 mm pass the bubble location and the camera catch the bubble collapse image process then record a cinematograph file. After this file is transfer to several sequence particle image data. Using the particle images and the PIV analysis method can obtain the velocity flow field feature during the bubble collapse process. Therefore, a single cavitation bubble and the subsequent bubble collapse flows induced by pressure waves are easily generated by the experimental setup proposed in this study. Cinematographic analysis of the cavitation bubble collapse flows at different stand-off distances are performed and discussed in the following.

3. Flow field measurement of the collapse of cavitation bubbles

It is found that the presence of the solid boundary has distinct influence on the flow field of a pressurized cavitation bubble and its final collapse. A distance parameter $\gamma=d/R_{MAX}$ (where R_{MAX} is the maximum radius and d is the distance between the bubble center and the solid boundary) is assigned to represent the distance from the center of the bubble to the solid boundary. When γ is in the range of $1 < \gamma \approx 3$, counter jet could be observed. However, no counter jet is generated under the condition of $\gamma > 3$. The results are described below:

3.1 Flow field measurement of bubble collapse at $\gamma \approx 7$

Under this condition, the distance between the center of the cavitation bubble and the solid boundary is nearly seven times of its radius. The flow field of the process of cavitation bubble collapse is not affected by the solid boundary. Therefore the solid boundary is assumed to be insignificant to the process of bubble collapse. This process of the cavitation bubble being pressurized followed by its final collapse is shown in Figure 3. The pressure wave is sent from the left side of the bubble surface, impacting the bubble with peak strength up to 155 kPa. The pressure wave caused a concaved deformation of the bubble shown in images from the first to the third rows of Figure 3.

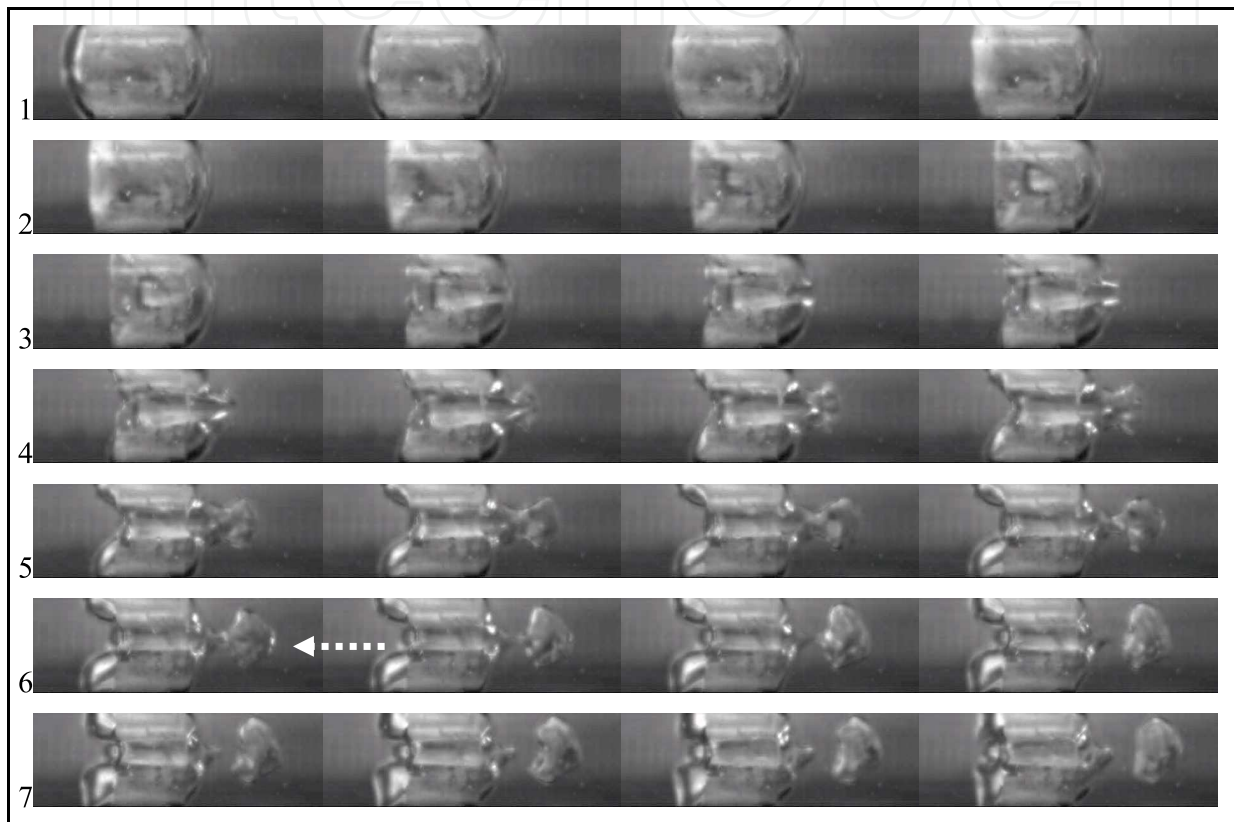


Fig. 3. Top view of images of the process of bubble collapse at $\gamma \approx 7$. From 1st row to 3rd row: image of the inward dent process; 4th and 6th rows: images of the Kelvin-Helmholtz vortex process (the Kelvin-Helmholtz vortex is indicated by a dotted line with an arrow). The peak strength of the pressure wave is 155 kPa. Image interval time is 1/4000 second. The size of each individual frame is 10.8 mm \times 3.1 mm. The bubble R_{\max} is 2.5 mm.

When sufficient energy is accumulated by the liquid jet during its continuous motion to the right side of the bubble, the overlaid surface is squeezed and subsequently spouted into a jet flow. When the jet flow extended to the static fluid at the right side of the bubble, rapid variation in the flow velocity is created which led to a Kelvin-Helmholtz vortex shown in images listed in images from the fourth to the sixth rows of Figure 3. Jaw et al. (2007) clearly described the Kelvin-Helmholtz vortex, indicating that the interaction between the pressure and the velocity variation is the main cause of this phenomenon.

The bubble collapse process is a complicated and three dimension flow structures. Using the 2D PIV analysis method was lacked a vertical direction motion measurement. In other word,

during the bubble surface was pressured to touch the solid boundary, the pressure is uniformly distributed across the tube area, the bubble deformation was approximate a symmetrical development condition. Under this condition, using a high speed camera and 2D PIV method could be obtained flow field. Figure 4 show the velocity flow field of the Kelvin-Helmholtz vortex formation process that used the PIV method to obtain flow field variation during the liquid jet to form vortex formation. The jet flow instantaneously spouted into the static fluid that cause between the jet flow and static fluid shear force difference increased, then the Kelvin-Helmholtz vortex formation is generated, as shown in Figure 4. From these series of images, the features of the cavitation bubble collapse without solid boundary effect are clearly manifested.

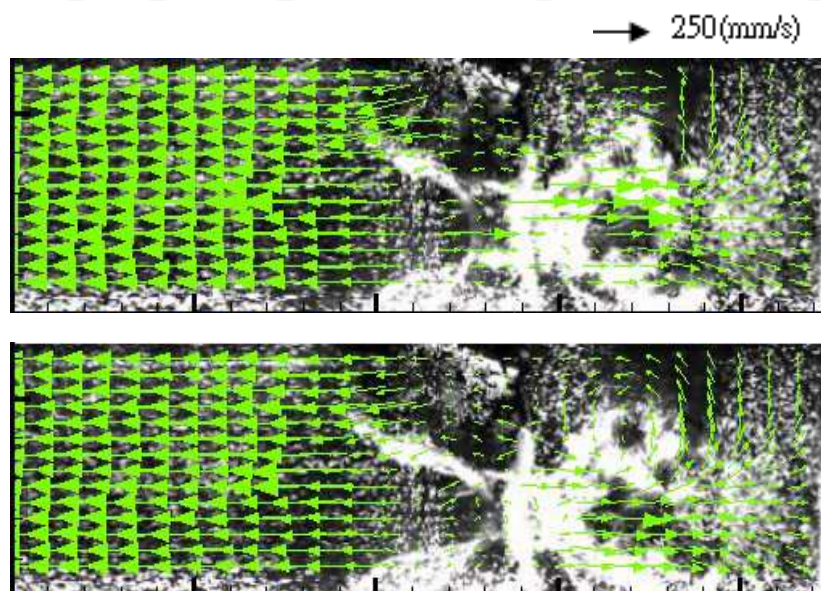


Fig. 4. Exhibit the PIV measurement results at $\gamma \approx 7$. (The velocity flow field of the Kelvin-Helmholtz vortex formation process) The peak strength of the pressure wave is 155 kPa. Image interval time is 1/4000 second. The size of each individual frame is 11.0 mm \times 3.1 mm. The bubble R_{\max} is 2.3 mm.

3.2 Flow field measurement of bubble collapse at $\gamma \approx 2$

As described in the introduction, the counter jet would be generated when the distance between the center of the bubble and the solid boundary is within one to three times the bubble's radius ($1 < \gamma \approx 3$). The experiments conducted with $\gamma \approx 2$ falls within this range.

The distance from the right side of the bubble surface to the solid boundary is only one radius long. The Kelvin-Helmholtz vortex was generated after the bubble surface is broken and the jet flow is formed. This vortex would touch the solid boundary and subsequently form the stagnation ring on the solid boundary shown in the left front view diagram in Figure 5. After the stagnation ring touched the solid boundary, it was divided into two fluid flows. One of them was outside the stagnation ring splashing outwardly along the radial direction. The other fluid flow inside the stagnation ring was squeezed inwardly along the central direction to form a counter jet shown in the lower right side of the diagram in Figure 5. The preexistence of fluid between the bubble surface and the solid boundary allowed the fluid inside the stagnation ring to be squeezed towards the center

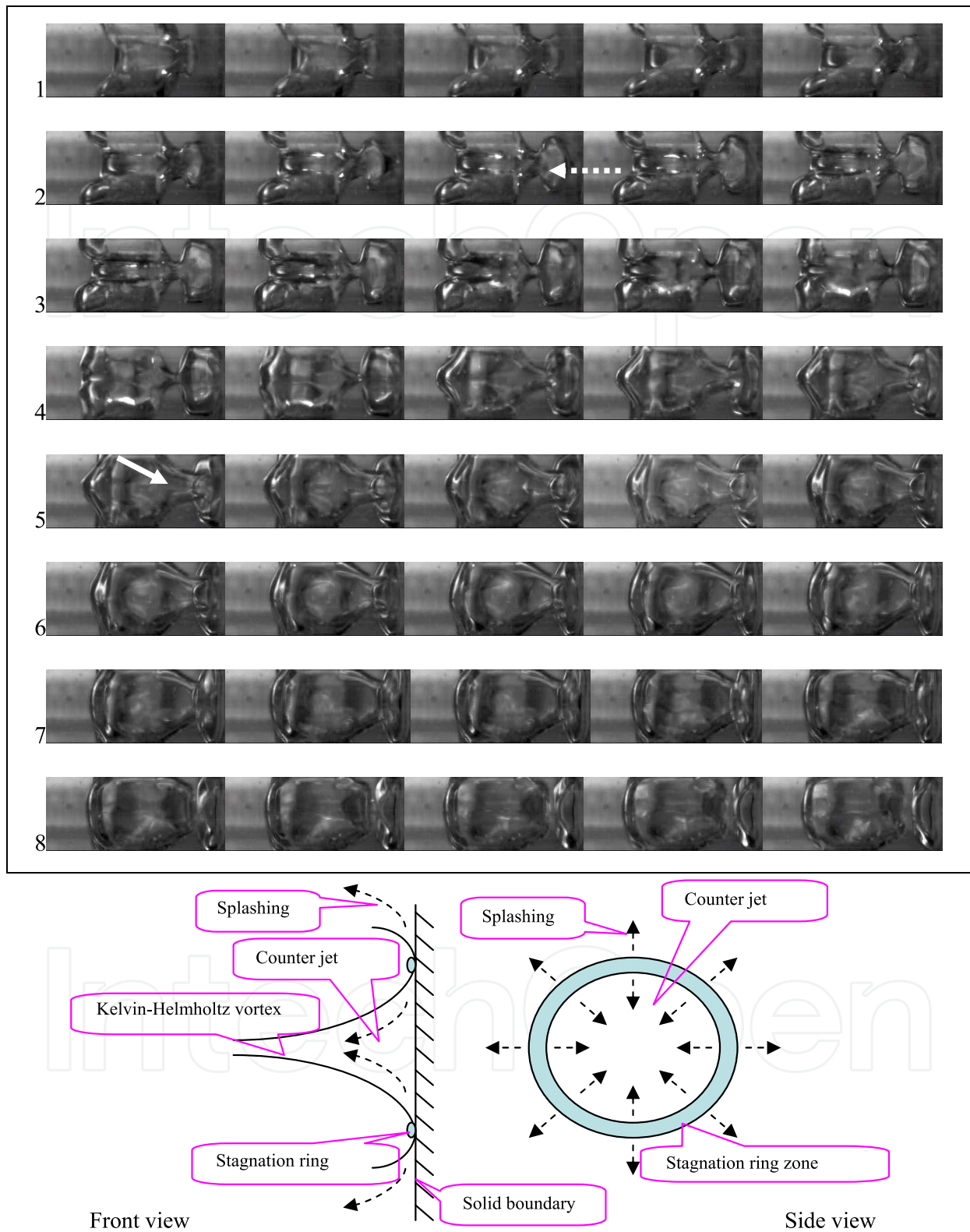


Fig. 5. Upper Part: The process of bubble collapse at $\gamma \approx 2$ (the Kelvin-Helmholtz vortex is indicated by a dotted line with an arrow, the counter jet indicated by a solid line with an arrow). The peak strength of the pressure wave is 250kPa. The image time interval is 1/4000 second. The size of each individual frame is 9.4mm \times 3.1 mm. R_{max} is 2.5mm. (Lower Part: sketch of Kelvin-Helmholtz vortex forming the counter jet.

resulting in a counter jet. Therefore in order to generate a counter jet, the bubble should be located at $\gamma > 1$ so that there would be enough space between the bubble surface and the solid boundary.

On the other hand, after the bubble surface was penetrated to form the Kelvin-Helmholtz vortex, a zone with high velocity and low pressure was formed at the root of the central axis of the vortex where the bubble was stretched and deformed towards its right side shown in images from the first to the third rows of Figure 5. In the first image at the fifth row of Figure 5, a counter jet located at the central axis of the bubble could be clearly seen.

Many researchers who studied the counter jet have mentioned the existence of the stagnation ring. However, in these studies, the time for the collapse of the bubble was too short for the appearance of the Kelvin-Helmholtz vortex. The relationship between the stagnation ring and the Kelvin-Helmholtz vortex was still not clear. In this study, the process for the formation of the Kelvin-Helmholtz vortex and the counter jet was clearly revealed for a shock wave of lower pressure was utilized to impact the cavitation bubble. If the strength of the pressure wave is increased, the resultant counter jet could penetrate the cavitation bubble and subsequently separated the bubble into a number of small bubbles as shown in Figure 6. In the second image at the fourth row of Figure 6 a counter jet located at the central axis of the bubble could be clearly seen.

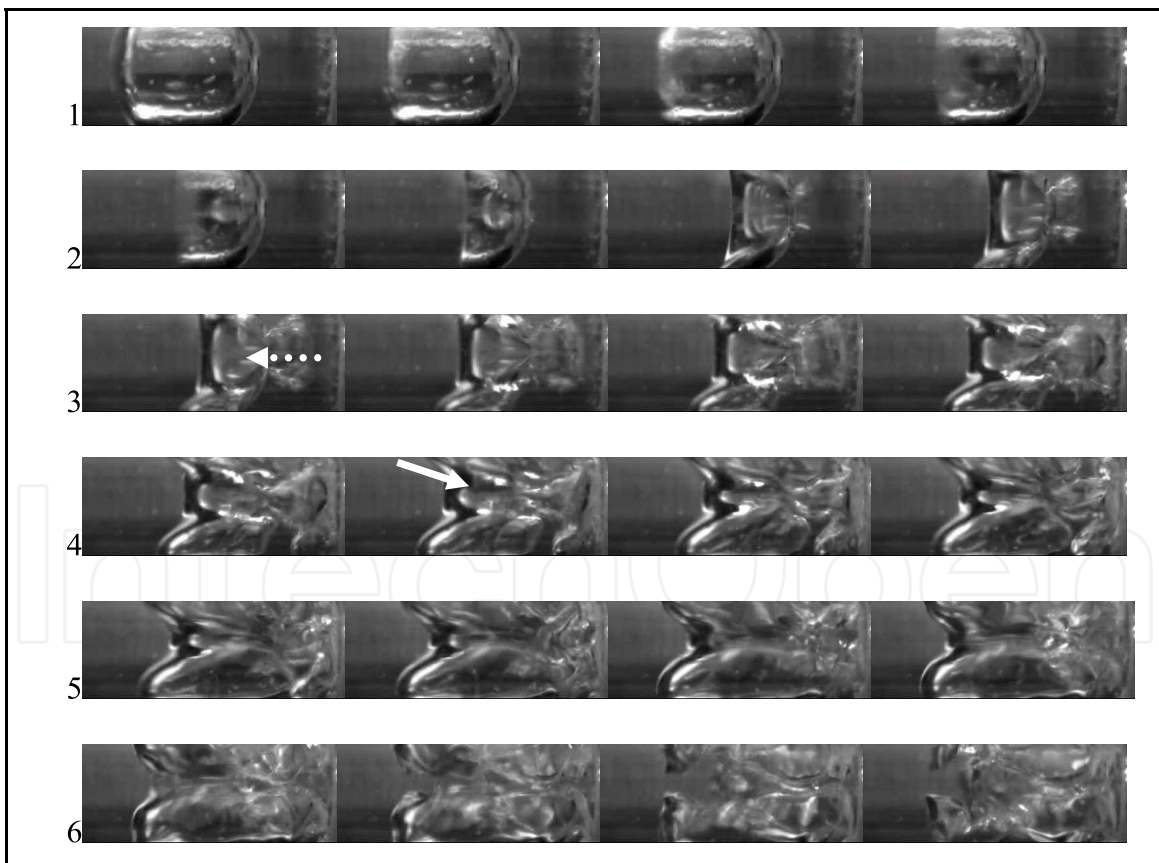


Fig. 6. Images of the process of bubble collapse at $\gamma \approx 2$ with image time interval of $1/4000$ second. The peak strength of the pressure wave is 405 kPa. The size of each individual frame is $9.8 \text{ mm} \times 3.1 \text{ mm}$ (the Kelvin-Helmholtz vortex is indicated by a dotted line with an arrow; the counter jet indicated by a solid line with an arrow). R_{max} is 2.5 mm.

Figure 7 show image and the velocity flow field from the Kelvin-Helmholtz vortex touch to the solid boundary and transfer to form the counter jet formation which used the PIV method to obtain velocity flow field variation. After the Kelvin-Helmholtz vortex touch solid boundary, the vortex is formed a planiform shape bubble along the solid boundary, and meantime the vortex formed a radial direction outward splashed out motion, as shown in upper left image and calculation result of Figure 7. Following by the bubble on the forward stretched effect and between the bubble and solid boundary space restriction conditions, the Kelvin-Helmholtz vortex at center part splash out are restricted and caused the velocity gradually decreased to stagnation at near the solid boundary center, as shown in upper right image and calculation result of Figure 7. Finally, the stagnation ring and counter jet are formed as shown in lower image and calculation results of Figure 7. They can be clear revealed that the stagnation ring location and counter jet motion that shown in Figure 8. The stagnation ring formation is located at a turning point of the velocity vectors

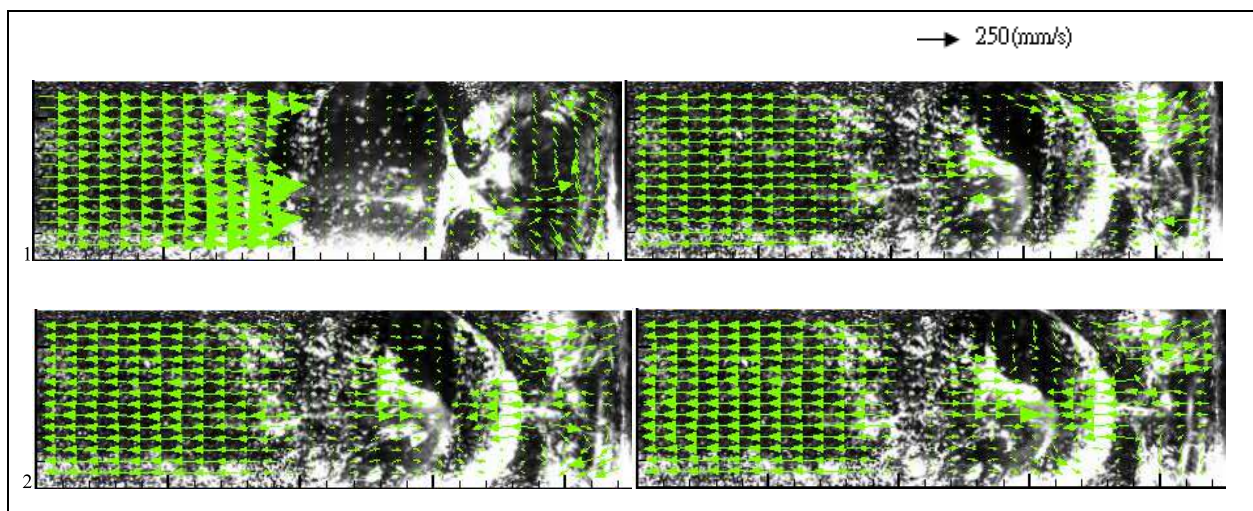


Fig. 7. Exhibit the PIV measurement results at $\gamma \approx 2$. (The velocity flow field of the Kelvin-Helmholtz vortex formation process) The peak strength of the pressure wave is 260 kPa. Image interval time is 1/4000 second. The size of each individual frame is 11.0 mm \times 3.1 mm. The bubble R_{max} is 2.3 mm.

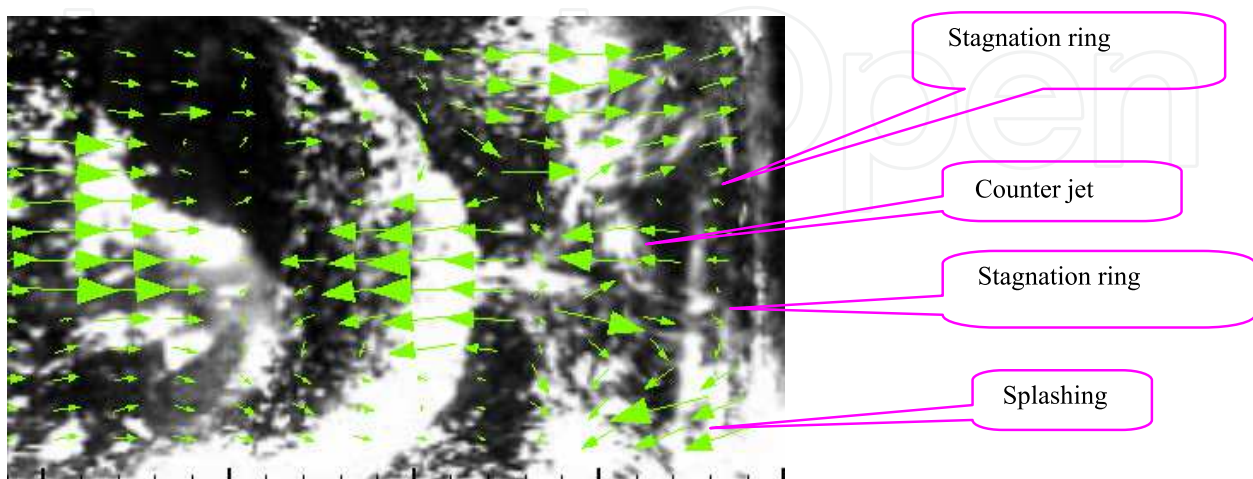


Fig. 8. The velocity flow field is the Figure 7 lower left diagram near solid boundary enlarged result that can reveal the stagnation ring location, splashing and the counter jet formation.

near the solid boundary. The counter jet formation is located at between two stagnation rings. The above-mentioned of the PIV calculation results reveal that the stagnation ring and the counter jet formation identically with Figure 5 lower part schematic diagram.

3.3 Flow field measurement of bubble collapse at $\gamma \approx 3$

The generation of the counter jet needs to satisfy the condition of $1 < \gamma \approx 3$. A critical value of $\gamma \approx 3$ is found to be a decisive value for the generation of a counter jet. In this study, three different strengths of pressure waves were used to trigger the breakdown the cavitation bubble. Flow field observation for this process of the collapse of cavitation bubble is carried out under this critical condition.

The images located at the first and second row of Figure 9 revealed the flow field of bubble collapse under a pressure wave of 200 kPa in strength. A liquid jet was formed followed by penetrating the bubble surface to produce the jet flow and the Kelvin-Helmholtz vortex. The bubble was divided into two small bubbles because the Kelvin-Helmholtz vortex did not touch the solid boundary. This process of collapse was similar to the case at $\gamma \approx 7$ where the counter jet was not generated.

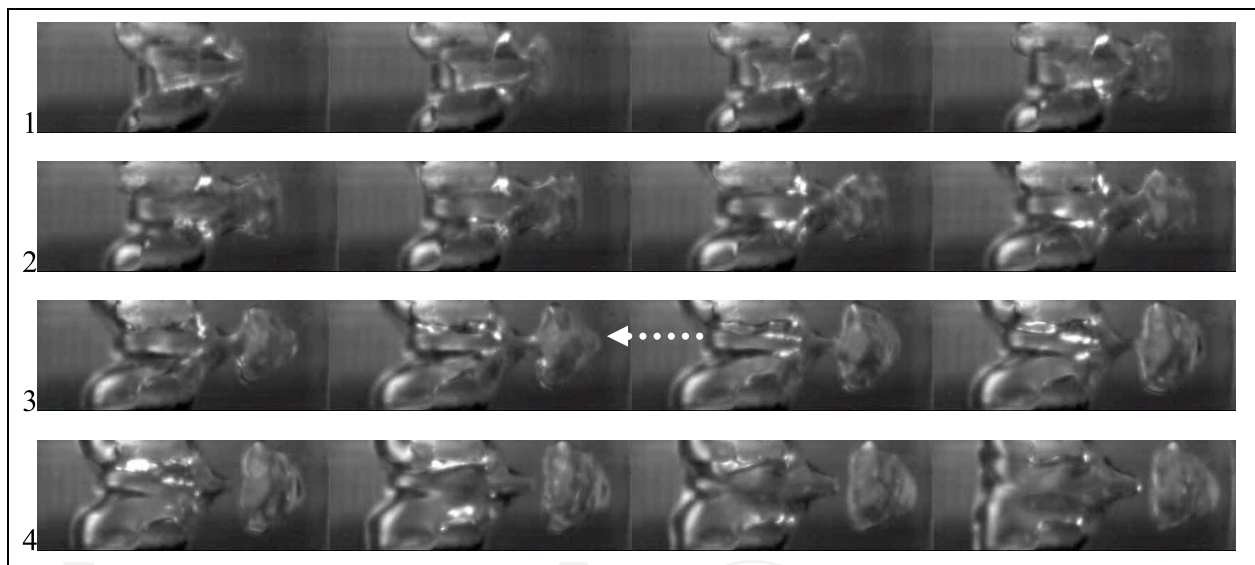


Fig. 9. Images of the process of bubble collapse at $\gamma \approx 3$. The peak strength of the pressure wave is 200 kPa. The size of each individual frame for is $10.5 \text{ mm} \times 3.1 \text{ mm}$, $R_{\text{max}} : 2.55 \text{ mm}$. The image time interval is $1/4000$ second. (The Kelvin-Helmholtz vortex is indicated by a dotted line with an arrow).

The process of the collapse of the bubble, with the strength of pressure wave increased to 300 kPa, is shown from the third to the sixth rows in Figure 10. Unlike the semi-hemispheric form of the Kelvin-Helmholtz vortex shown in the third row of Figure 9, the vortex shown here was clearly influenced by the solid boundary when the liquid jet penetrated the bubble surface. The right side of the head of the vortex touched the solid boundary and turned into a planiform shape before splashing and spreading outwardly along its surrounding interface. On the other hand, before the head of the vortex touched the solid boundary, the outer ring of the vortex had already touched the tube wall and started spreading outwardly shown in the images at the first row in Figure 10. This spreading vortex kept



Fig. 10. Images of the process of bubble collapse at $\gamma \approx 3$. The peak strength of the pressure wave is 300kPa. The size of each individual frame is 9.6 mm \times 3.1 mm. R_{\max} : 2.35 mm. The image time interval is 1/4000 second. (The Kelvin -Helmholtz vortex is indicated by a dotted line with an arrow).

moving towards the right side until it touched the solid boundary and generated a subsequent shock wave which rebounded to produce the phenomenon of Richtmyer-Meshkov instability shown near the solid boundary in every image from the second to the third rows of Figure 10. Although the Kelvin-Helmholtz vortex could be generated under this strength of pressure wave, the vortex had already splashed and touched the surrounding solid boundary, disabling the vortex from forming the stagnation ring and the counter jet. At the end of this process, the bubble was divided by the liquid jet and the root of the vortex into two smaller bubbles shown in the images from the fifth to seventh rows in Figure 10.

If the strength of the pressure wave is increased to a peak value of 365 kPa, the Kelvin-Helmholtz vortex would touch the solid boundary before the formation of the stagnation ring and the counter jet. This process is shown in the image listed at the 5th and 6th rows of Figure 11.



Fig. 11. Images of the process of bubble collapse at $\gamma \approx 3$. The peak strength of the pressure wave is 365 kPa. The size of each individual frame is 2.25 mm. The image time interval is 1/4000 second. (The Kelvin-Helmholtz vortex is indicated by a dotted line with an arrow; the counter jet is indicated by a solid line with an arrow).

3.4 Flow field measurement of bubble collapse at $\gamma \approx 1$ and $\gamma = 1$

The other critical value for the formation of the counter jet occurs at $\gamma \approx 1$ where the bubble is tightly close to the solid boundary. In this study, in order to understand the characteristics of the flow fields under this critical condition, measurements of flow fields at both locations where γ is slightly greater than and equal to one were carried out.

1. When the bubble is located at γ slightly greater than 1, there would be a small distance between the bubble surface and the rigid boundary. When the bubble was pressurized and concaved inward, the bubble became more planiform in shape for this deformation was caused by the solid boundary. The area of inward concaved bubble is larger than

the three cases mentioned before shown in Figure 12. After the liquid jet penetrated the bubble surface, there is not enough space to form a complete Kelvin-Helmholtz vortex. However, the space between the bubble surface and the solid boundary would still exist a gap allow the formation of stagnation ring after the liquid jet touches the solid boundary. This is followed by an outward splash along the radial direction while the inward stagnation ring was squeezed along the central direction to form the counter jet. Finally the bubble was divided into two smaller bubbles by the counter jet shown in the image of Figure 12 and diagram in Figure 13. In the further, using PIV calculation results shown in Figure 14. This result are clear revealed that the liquid jet direct touch the solid boundary and then form the stagnation ring and the counter jet formation.

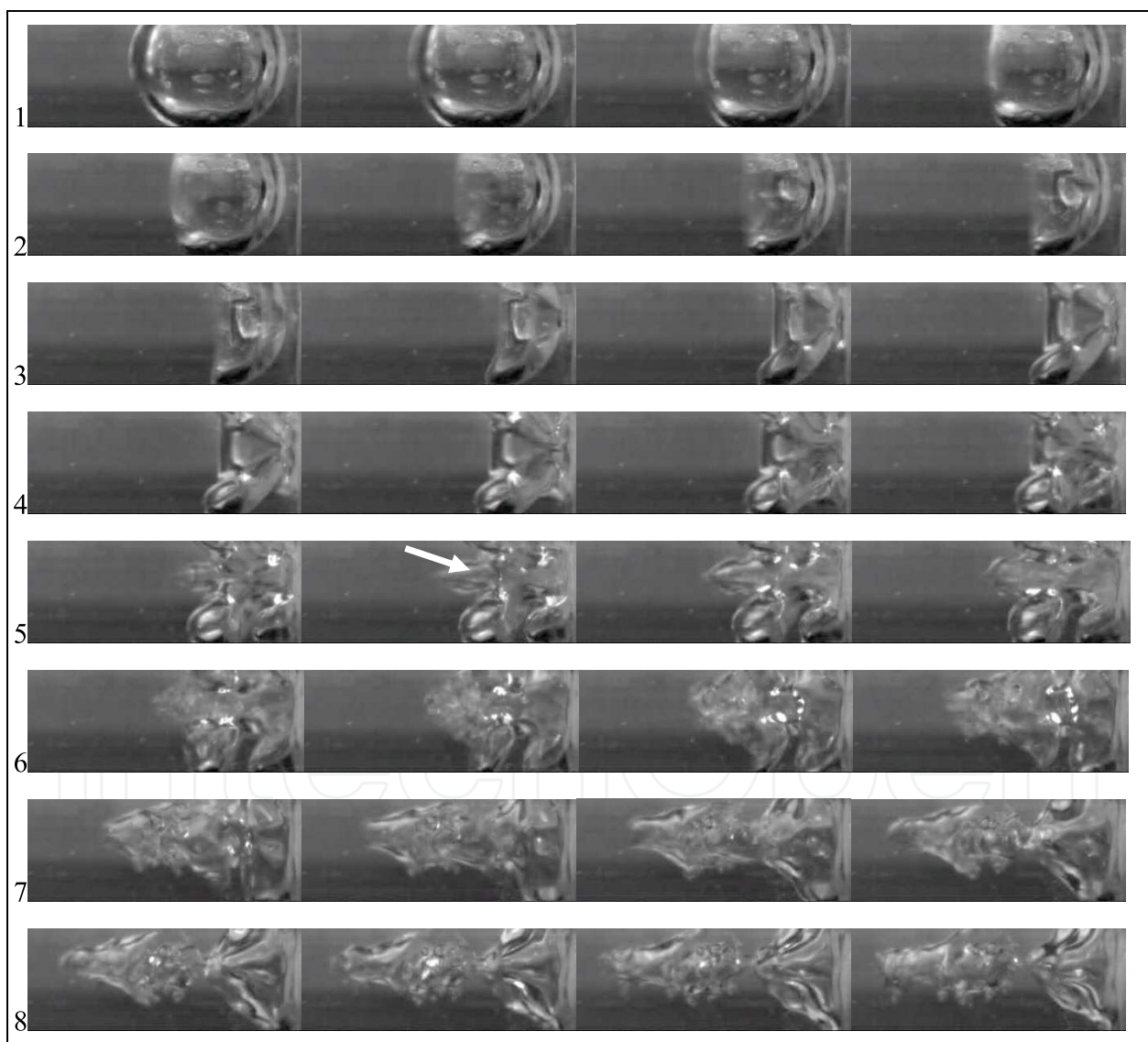


Fig. 12. Images of the process of bubble collapse at $\gamma = 1$; the peak strength of the pressure wave is 325 kPa; the image time interval is 1/4000 second. The size of each individual frame is 8.3mm \times 3.1 mm. R_{\max} is 2.4 mm. (The counter jet is indicated by a solid line with an arrow).

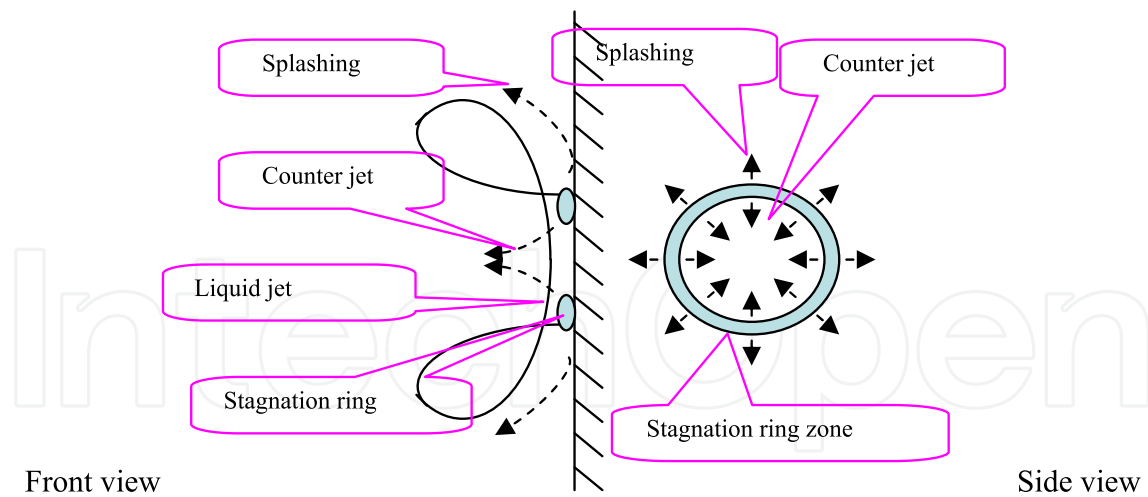


Fig. 13. sketch of the liquid jet position. (Note: Left diagram: the solid line is the bubble surface and the dotted line with an arrow is the splashing.)

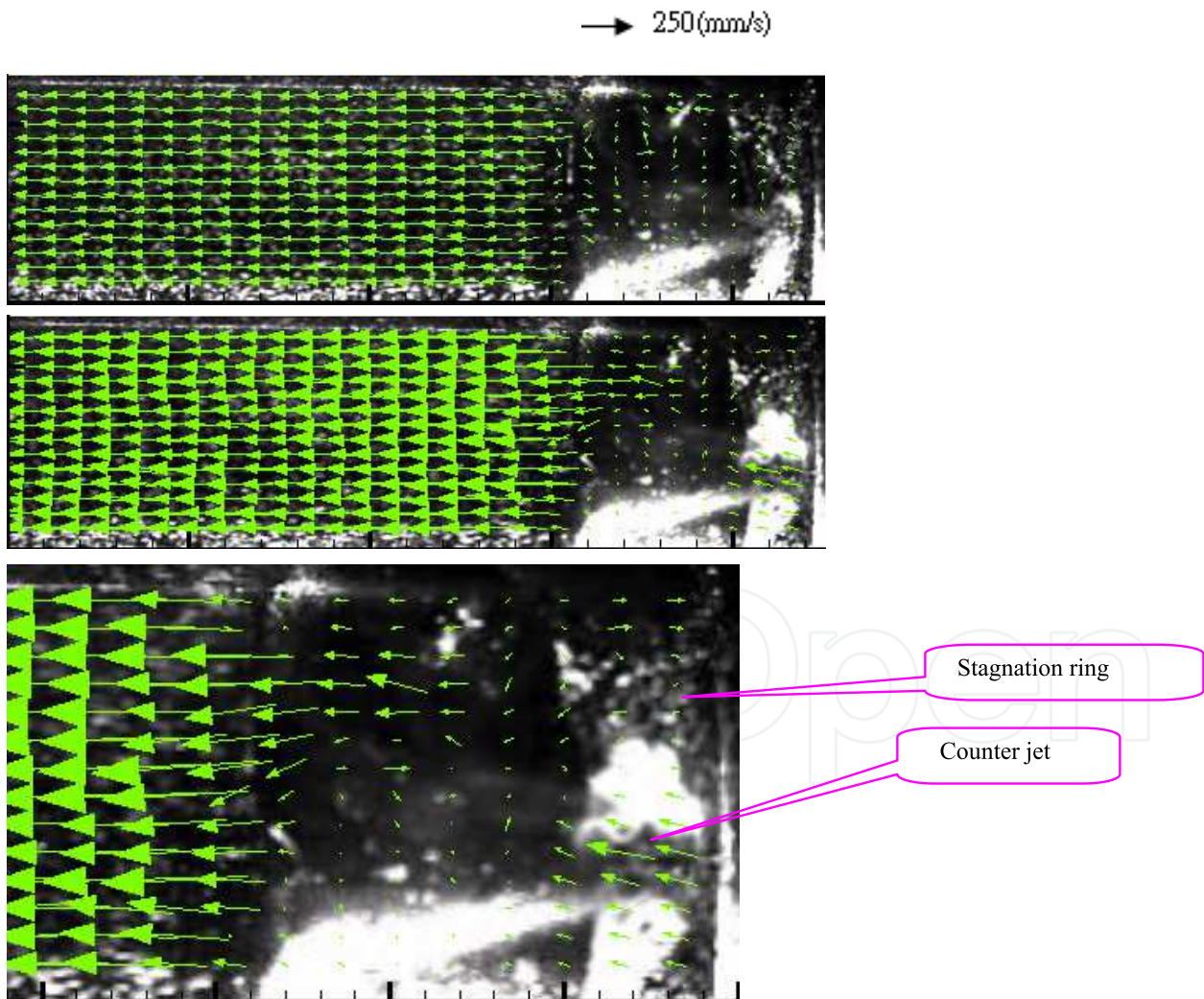


Fig. 14. Upper Part: exhibit the PIV measurement results at $\gamma \approx 1$. The peak strength of the pressure wave is 320 kPa. Image interval time is 1/4000 second. The size of each individual frame is 8.8.0 mm \times 3.1 mm. The bubble R_{\max} is 2.4 mm. Lower part: exhibit

the upper right diagram near solid boundary enlarged the result that can reveal the stagnation ring location and the counter jet formation. (Note: the velocity vectors near the solid boundary are the particle motion results, not from the solid boundary extra velocity boundary condition).

2. Under the condition of $\gamma = 1$, the bubble interface was pressurized to form an inward concaved bubble. It was followed by the overlaying of the bubble interfaces on the solid boundary without any spaces left for the fluid. After the liquid jet impacted the solid boundary, it just moved outwardly as a splash along the radial direction. The bubble collapses subsequently on the radial trajectory without forming of the stagnation ring and the inwardly squeezed counter jet. This process of bubble collapse is shown in the images and diagrams in Figure 15.



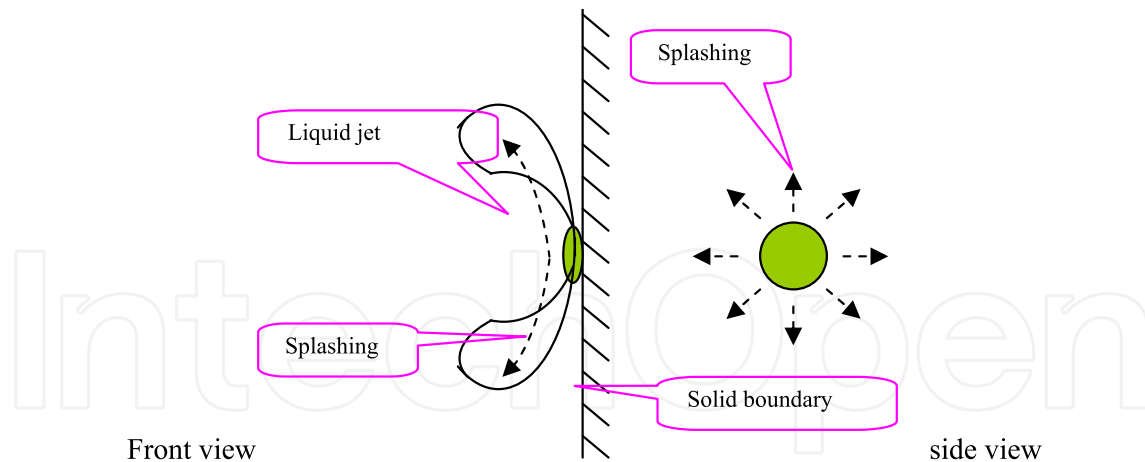


Fig. 15. Images of the process of bubble collapse at $\gamma = 1$; the peak strength of the pressure wave is 520 kPa; the image time interval is 1/4000 second. The size of each individual frame is 6.2 mm \times 3.1 mm. R_{\max} is 2.25 mm. Lower Part: sketch of the liquid jet position.

4. Conclusions

This study utilized a U-shape platform device to generate a single cavitation bubble and sequential images of the bubble collapse flow are recorded by a high speed camera for the detail analysis of the flow field characteristics and the cause of the counter jet during the process of bubble collapse induced by pressure wave. A series of bubble collapse flows induced by pressure waves of different strengths are investigated by positioning the cavitation bubble at different stand-off distances to the solid boundary. It is found that the Kelvin-Helmholtz vortices are formed when the liquid jet induced by the pressure wave penetrates the bubble surface. If the bubble center to the solid boundary is within one to three times the bubble's radius, a stagnation ring will form on the boundary when impacted by the penetrated jet. The liquid inside the stagnation ring is squeezed toward the center of the ring to form a counter jet after the bubble collapses. At the critical position, where the bubble center from the solid boundary is about three times the bubble's radius, the bubble collapse flows will vary. Depending on the strengths of the pressure waves applied, either just the Kelvin-Helmholtz vortices form around the penetrated jet or the penetrated jet impacts the boundary directly to generate the stagnation ring and the counter jet flow. This phenomenon used the particle image velocimetry method can be clearly revealed the flow field variation of the counter jet. If the bubble surface is in contact with the solid boundary, the liquid jet can only splash radially without producing the stagnation ring and the counter jet.

For all the experiments performed in this study, the strength of the pressure wave adopted to induce the bubble collapse flow was kept as low as possible so that the bubble collapsed in a longer period of time. The characteristics of the bubble collapse flows at different stand-off distances can thus be clearly manifested. However, different strengths of the pressure waves are needed to induce the bubble collapse flow at different γ locations. A lower strength of the pressure wave is needed for an increasing γ value and vice versa.

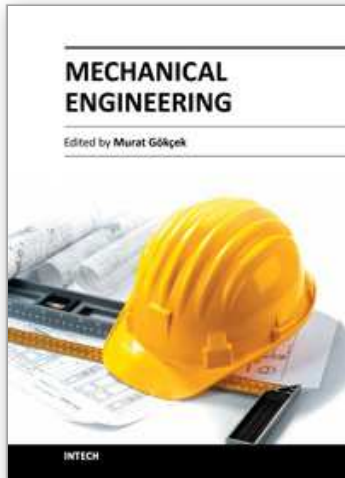
5. References

- Akmanov, A. G., Ben'kovskii, V. G., Golubnichii, P. I., Maslennikov, S. I., and Shemanin, V. G. (1974). Laser sonoluminescence in a liquid, *Soviet Physics Acoustics*, 19, pp.417-418.

- Benjamin, T. B. and Ellis, A. T. (1966). The collapse of cavitation bubbles and the pressures thereby produced against solid boundaries, *Philosophical Transactions of the Royal Society of London Series A, Mathematical and Physical Sciences*, 260, pp221-240.
- Best, J. P. (1993). The formation of toroidal bubbles upon the collapse of transient cavities, *Journal of Fluid Mechanics*, 251, pp.79-107.
- Blake, J. R., Hooton, M. C., Robinson, P. B. and Tong, R. P. (1997). Collapsing cavities, toroidal bubbles and jet impact, *Philosophical Transactions Mathematical, Physical and Engineering Sciences*, 355, pp.537-550.
- Buzukov, A. A. and Teslenko, V. S. (1971). Sonoluminescence following focusing of laser radiation into liquid, *Journal of Experimental and Theoretical Physics Letters*, 14, pp. 189-191.
- Harrison, M. (1952). An experimental study of single bubble cavitation noise, *The Journal of the Acoustical Society of America*, 24, pp.776-782.
- Jaw, S. Y., Chen, C. J. and Hwang, R. R. (2007), Flow visualization of bubble collapse flow, *Journal of Visualization*, 10, pp.21-24.
- Kling, C. L. and Hammitt, F. G. (1972). A photographic study of spark-induced cavitation bubble collapse, *Transactions of the ASME D: Journal of Basic Engineering*, 94, pp.825-833.
- Kodama, T. and Tomita, Y., (2000). Cavitation bubble behavior and bubble-shock wave interaction near a gelatin surface as a study of in vivo bubble dynamics, *Applied Physical B*, 70, pp.139-149.
- Kornfeld, M. and Suvorov, L. (1944). On the destructive action of cavitation, *Journal of Applied Physics*, 15, pp.495-506.
- Lauterborn, W. (1974). Kavitation durch laserlicht, *Acustica*, 31, pp.52-78 .
- Lauterborn, W. (1972). High-speed photography of laser-induced breakdown in liquids, *Applied Physical Letters*, 21, pp. 27-29.
- Lawson, N. J., Rudman, A. Guerra, J. and Liow, J. L. (1999). Experimental and numerical comparisons of the break-up of a large bubble, *Experiments in fluids*, 26, pp.524-534.
- Lindau, O. and Lauterborn, W. (2003). Cinematographic observation of the collapse and rebound of a laser-produced cavitation bubble near a wall, *Journal of Fluid Mechanics*, 479, pp.327-348.
- Plesset, M. S. (1949). The dynamics of cavitation bubbles, *Trans. ASME: Journal of Applied Mechanics*, 16, pp.277-282.
- Naude, C. F. and Elli, A. T. (1961). On the mechanism of cavitation damage by nonhemispherical cavities collapse in contact with a solid boundary, *Transactions of the ASME D: Journal of Basic Engineering*, 83, pp.648-656.
- Ohl, C. D., Philipp, A., and Lauterborn, W. (1995). Cavitation bubble collapse studied at 20 million frames per second, *Annalen der Physik*, 4, pp.26-34.
- Ohl, C. D., Lindau, O. and Lauterborn, W. (1998). Luminescence from spherically and aspherically collapsing laser induced bubbles, *Physical Review Letters*, 80, pp.393-397.
- Plesset, M. S. and Chapman, R. B. (1971). Collapse of an initially spherical vapour cavity in the neighbourhood of a solid boundary, *Journal of Fluid Mechanics*, 47, pp.283-290.
- Philipp, A., Delius, M., Scheffczyk, C., Vogel, A. and Lauterborn, W. (1993). Interaction of lithotripter-generated shock waves with air bubbles, *The Journal of the Acoustical Society of America*, 93, pp.2496-2509.

- Philipp, A. and Lauterborn, W. (1998). Cavitation erosion by single laser-produced bubbles, *Journal of Fluid Mechanics*, 361, pp.75-116.
- Raleigh, L., (1917). On the pressure developed in a liquid during the collapse of a spherical cavity, *Philosophical Magazine*, 34, pp.94-98.
- Sankin, G. N., Simmons, W. N., Zhu, S. L. and Zhong, P. (2005). Shock wave interaction with laser-generated single bubble, *Physical Review Letter*, 034501, pp. 1-4.
- Shaw, S. J., Jin, Y. H., Schiffers, W. P. and Emmony, D. C. (1996). The interaction of a single laser-generated cavity in water with a solid surface, *The Journal of the Acoustical Society of America*, 99, pp.2811-2824.
- Tomita, Y. and Shima, A. (1986). Mechanisms of impulsive pressure generation and damage pit formation by bubble collapse, *Journal of Fluid Mechanics*, 169, pp.535-564.
- Vogel, A. and Lauterborn, W. (1988). Time-resolved particle image velocimetry used in the investigation of cavitation bubble dynamics, *Applied Optics*, 29, pp.1869-1876.
- Vogel, A., Lauterborn, W. and Timm, R. (1989). Optical and acoustic investigations of the dynamics of laser-produced cavitation bubbles near a solid boundary, *Journal of Fluid Mechanics*, 206, pp.299-338.
- Ward, B. and Emmony, D. C. (1991). Direct observation of the pressure developed in a liquid during cavitation-bubble collapse, *Applied Physics Letters*, 59, pp.2228-2231.
- Zhang, S. Duncan, J. H. and Chahine, G.L. (1993). The final stage of the collapse of a cavitation bubble near a rigid wall, *Journal of Fluid Mechanics*, 257, pp.147-181.
- Zhu, S. and Zhong, P. (1999). Shock wave-inertial microbubble interaction: A theoretical study based on the Gilmore formulation for bubble dynamics, *The Journal of the Acoustical Society of America*, 106, pp.3024-2033.

IntechOpen



Mechanical Engineering

Edited by Dr. Murat Gokcek

ISBN 978-953-51-0505-3

Hard cover, 670 pages

Publisher InTech

Published online 11, April, 2012

Published in print edition April, 2012

The book substantially offers the latest progresses about the important topics of the "Mechanical Engineering" to readers. It includes twenty-eight excellent studies prepared using state-of-art methodologies by professional researchers from different countries. The sections in the book comprise of the following titles: power transmission system, manufacturing processes and system analysis, thermo-fluid systems, simulations and computer applications, and new approaches in mechanical engineering education and organization systems.

How to reference

In order to correctly reference this scholarly work, feel free to copy and paste the following:

Sheng-Hsueh Yang, Shenq-Yuh Jaw and Keh-Chia Yeh (2012). Experimental Study on Generation of Single Cavitation Bubble Collapse Behavior by a High Speed Camera Record, Mechanical Engineering, Dr. Murat Gokcek (Ed.), ISBN: 978-953-51-0505-3, InTech, Available from:

<http://www.intechopen.com/books/mechanical-engineering/experimental-study-on-generation-of-single-cavitation-bubble-collapse-behavior-by-a-high-speed-camer>

INTECH
open science | open minds

InTech Europe

University Campus STeP Ri
Slavka Krautzeka 83/A
51000 Rijeka, Croatia
Phone: +385 (51) 770 447
Fax: +385 (51) 686 166
www.intechopen.com

InTech China

Unit 405, Office Block, Hotel Equatorial Shanghai
No.65, Yan An Road (West), Shanghai, 200040, China
中国上海市延安西路65号上海国际贵都大饭店办公楼405单元
Phone: +86-21-62489820
Fax: +86-21-62489821

© 2012 The Author(s). Licensee IntechOpen. This is an open access article distributed under the terms of the [Creative Commons Attribution 3.0 License](#), which permits unrestricted use, distribution, and reproduction in any medium, provided the original work is properly cited.

IntechOpen

IntechOpen